VIR-Dawn Observations of Ceres at Low Phase Angles. M. Ciarniello[1], M. C. De Sanctis[1], E. Ammannito[2], A. Raponi[1], F. G. Carrozzo[1], A. Longobardo[1], F. Tosi[1], E. Rognini[1], F. Zambon[1], C. A. Raymond[3], C. T. Russell[4]. [1]IAPS-INAF (via del Fosso del Cavaliere, 100, 00133, Rome, Italy; mauro.ciarniello@iaps.inaf.it), [2]ASI, Rome, Italy, [3]Jet Propulsion Laboratory, California Institute of Technology, Pasadena, CA, USA, [4]University of California Los Angeles, Earth Planetary and Space Sciences, Los Angeles, CA, USA

Introduction: The Visible and InfraRed mapping spectrometer (VIR) [1] onboard the NASA Dawn mission performed an extensive observation campaign of the surface of Ceres in the 0.25-5.1 μm spectral interval. Previous observations were performed in the phase angle range 7°-132°, allowing the characterization of a large part of Ceres' phase curve, with the exception of the Opposition Effect (OE) region [2]. OE represents a surge of the reflectance at small phase angles, commonly observed in atmosphereless bodies [3,4,5]. Recent acquisitions obtained by the Dawn mission on 29 April 2017 during the Extended Mapping Orbit 4 (XMO4) mission phase allowed to observe Ceres' surface down to ~0° phase angle, permitting the characterization of the OE region with VIR. Here we report about preliminary results from the analysis of these observations.

Data Set: the VIR instrument acquired 19 hyperspectral cubes during XMO4 phase by means of the VIS channel (0.25-1.05 μm) and 1 hyperspectral cube with the IR channel (1.0-5.1 μm) characterizing the ~0°-6.5° and ~0°-1.6° phase angle ranges, respectively. The typical spatial resolution of this set of observations is ~5 km/pixel.

Hapke model of Ceres' reflectance: In [2] Ceres' spectrophotometric properties have been investigated by means of a simplified Hapke model [3] following the formulation reported in the equation below:

$$\frac{I}{F} = \frac{w}{4}\frac{\mu_{0eff}}{\mu_{0eff}+\mu_{eff}}\left[\left(1+B(\alpha)\right)p(\alpha) + H\left(w,\mu_{0eff}\right)H\left(w,\mu_{eff}\right)-1\right]S(i,e,\alpha,\bar{\theta}) \quad \text{Eq. 1}$$

with

w: single scattering albedo.

α,i,e: phase, incidence and emission angles, respectively.

p(α): single particle phase function (SPPF) modeled with a two-parameter Henyey-Greenstein formulation [3].

B(α): Shadow hiding OE function depending on OE amplitude (B_0) and angular width (h).

$S(i,e,\alpha,\bar{\theta})$: large scale roughness shadowing function, depending on the average surface roughness slope $\bar{\theta}$.

*H(w,x):*Chandrasekhar function.

μ_{0eff}, μ_{eff}: cosine of the effective incidence and emission angle, respectively.

Assuming Eq. 1, this can be rearranged as follows:

$$\frac{I/F}{D} = \frac{w}{8}\left[\left(1+B(\alpha)\right)p(\alpha) + H\left(w,\mu_{0eff}\right)H\left(w,\mu_{eff}\right)-1\right] \quad \text{Eq. 2}$$

where $D = \frac{\mu_{0eff}+\mu_{eff}}{2\mu_{0eff}}\frac{1}{S(i,e,\alpha,\bar{\theta})}$

We refer to the quantity $\frac{I/F}{D}$ reported in Eq. 2 as Ceres' "phase function" since it is mostly dependent on phase angle, while, given the low albedo of Ceres' surface, dependence on incidence and emission angle through the *H* functions is small. In this analysis, the study of Ceres' spectrophotometric properties performed in [2] is extended at low phase angles by means of XMO4 observations. In Fig. 2, we show Ceres' phase function as derived from VIR after averaging in phase angles bins (0.2° bins for α<7°, 1° bins for α>7°) and normalization at 0°. It can be noted that Ceres' phase function is progressively more forward-scattering for increasing wavelengths.

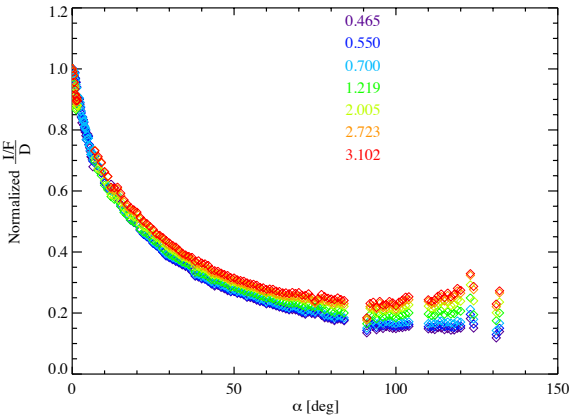

Figure 1. Top panel: Ceres' phase function at different wavelengths (expressed in μm) indicated in the plot, after normalization at 0° phase angle.

SHOE and CBOE: OE in regolith is typically ascribed to two different mechanisms [3 and references therein]: Shadow Hiding Opposition Effect (SHOE) and Coherent Backscattering Opposition Effect (CBOE). The first is due to the reducing visibility of the shadows cast by particles in the top layers on the ones below when phase angle decreases, while CBOE is due to the constructive interference at low phase angles between waves propagating in the medium along the same path but in opposite directions. SHOE is typically characterized by an angular width up to ~10°-20° which does not

depend on wavelength [3], being mainly driven by light singly scattered in the medium. On the other hand, CBOE is related to multiple scattering and its angular width, which is typically smaller than SHOE (~1°-2°, [3,4]), is a function of wavelength. In Fig. 2, Ceres' phase curve at small phase angles (top panel: α<10°; bottom panel: α<2°) is shown at different wavelengths. It can be noted that there is no clear spectral dependence of the OE angular width. The observed variability for α<2°, in particular at IR wavelengths, is most likely related to the fact that different phase angles sample different regions of the surface, because of the poor observations redundancy. Although an unambiguous assessment of CBOE requires polarimetry measurements [5], this suggests SH as the principal mechanism producing OE on Ceres, and it is compatible with the adoption of Eq. 1, which neglects CBOE.

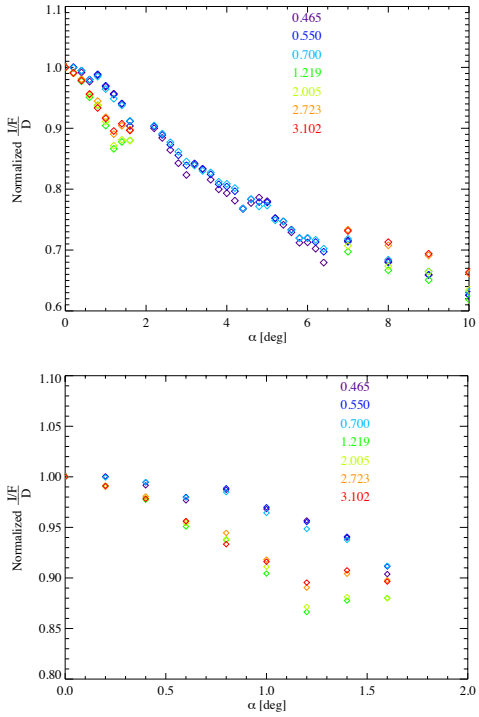

Figure 2. Top panel: Ceres' phase function in the 0°-10° phase angle range at different wavelengths (expressed in μm) indicated in the plot, after normalization at 0° phase angle. Bottom panel: zoom of the 0°-2° phase angle interval.

Hapke's model parameters:
Taking advantage of the extended phase angle coverage provided by XMO4 observations it is possible to derive improved sets of Hapke's model parameters with respect to [2] across the whole investigated spectral range, by fitting the phase function to Eq. 2. Various solutions have been investigated, depending on different a priori assumptions on Hapke's model parameters. For example, assuming that B_0 cannot exceed 1, as required from SHOE, and $\bar{\theta}$=29° from [2] we derive the following preliminary solution at 0.55 μm with *B_0=1, h=0.037, b=0.40 c=0.23, w=0.15*. In this case, the derived single scattering albedo is representative of a low albedo surface, while the values for *b* and *c* are compatible with particles characterized by an intermediate level of internal scatterers, according to the classification proposed by [6]. Finally, the SHOE angular width (*h*) can be related to the porosity (*P*) of the regolith (Eq. 9.26 in [3]) and the derived value corresponds to *P*=0.91, indicating a relatively large porosity.

Monte Carlo simulations: With the aim to further characterize the porosity of the surface, we perform a preliminary comparison of Ceres' reflectance curve as computed at selected observations geometries from the derived Hapke's model, with Monte Carlo (MC) ray-tracing simulations [7] in regolith. MC simulations have been performed for different filling factors of the modeled regolith Φ=0.01-0.05-0.1-0.2-0.3 (Fig.3). It can be noted that larger filling factors provide larger OE widths, and Ceres' reflectance curve is better matched by MC simulations with Φ between 0.05-0.1, (P=0.9-0.95), which is compatible with the result derived from the fitting of Hapke's model.

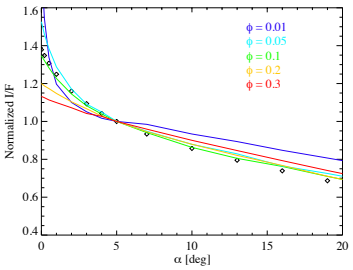

Figure 3. MC simulations (solid curves) for different Φ, compared to simulated I/F of Ceres's surface with Hapke's theory (diamonds). For all the simulated observations geometries we assumed i=0° and e=α.

References: [1] De Sanctis, M. C. et al. (2011), *Space Sci. Rev., 163, 329*. [2] Ciarniello, M. et al. (2017), *A&A 598*, A130. [3] Hapke B.W. (2012), *Theory of reflectance and emittance spectroscopy*. [4] M. Mishchenko (1992), *Astrophys. Space Sci.* 194, 327–333. [5] Nelson et al. (2000), *Icarus, 147, 545–558*. [6] McGuire A. F. and Hapke B. W. (1995), *Icarus 113, 134-155*. [7] Ciarniello et al., (2014). *Icarus 237, 293–305*

Acknowledgements: This work is supported by the Italian Space Agency (ASI, ASI-INAF n. I/004/12/1) and NASA. Enabling contributions from the Dawn Instrument, Operations, and Science Teams are gratefully acknowledged.